

---

# Flexible Heteroscedastic Count Regression with Deep Double Poisson Networks

---

**Spencer Young**

Delicious AI  
spencer.young@deliciousai.com

**Porter Jenkins**

Computer Science Department  
Brigham Young University  
pjenkins@cs.byu.edu

**Longchao Da**

School of Computing and Augmented Intelligence  
Arizona State University  
longchao@asu.edu

**Jeff Dotson**

Marketing Department  
Ohio State University  
dotson.83@osu.edu

**Hua Wei**

School of Computing and Augmented Intelligence  
Arizona State University  
hua.wei@asu.edu

## Abstract

Neural networks that can produce accurate, input-conditional uncertainty representations are critical for real-world applications. Recent progress on heteroscedastic *continuous* regression has shown great promise for calibrated uncertainty quantification on complex tasks, like image regression. However, when these methods are applied to *discrete* regression tasks, such as crowd counting, ratings prediction, or inventory estimation, they tend to produce predictive distributions with numerous pathologies. We propose to address these issues by training a neural network to output the parameters of a Double Poisson distribution, which we call the Deep Double Poisson Network (DDPN). In contrast to existing methods that are trained to minimize Gaussian negative log likelihood (NLL), DDPNs produce a proper probability mass function over discrete output. Additionally, DDPNs naturally model under-, over-, and equi-dispersion, unlike networks trained with the more rigid Poisson and Negative Binomial parameterizations. We show DDPNs 1) vastly outperform existing discrete models; 2) meet or exceed the accuracy and flexibility of networks trained with Gaussian NLL; 3) produce proper predictive distributions over discrete counts; and 4) exhibit superior out-of-distribution detection. DDPNs can easily be applied to a variety of count regression datasets including tabular, image, point cloud, and text data.

## 1 Introduction

The pursuit of neural networks capable of learning accurate and reliable uncertainty representations has gained significant traction in recent years [1, 2, 3, 4]. Input-dependent uncertainty is useful for detecting out-of-distribution data [5, 6, 7], active learning [8, 9], reinforcement learning [10, 11], and real-world decision-making under uncertainty [12]. While uncertainty quantification applied to regression on continuous outputs is well-studied, training neural networks to make probabilistic predictions over discrete counts has traditionally received less attention, despite multiple relevant applications. In recent years, neural networks have been trained to predict the size of crowds

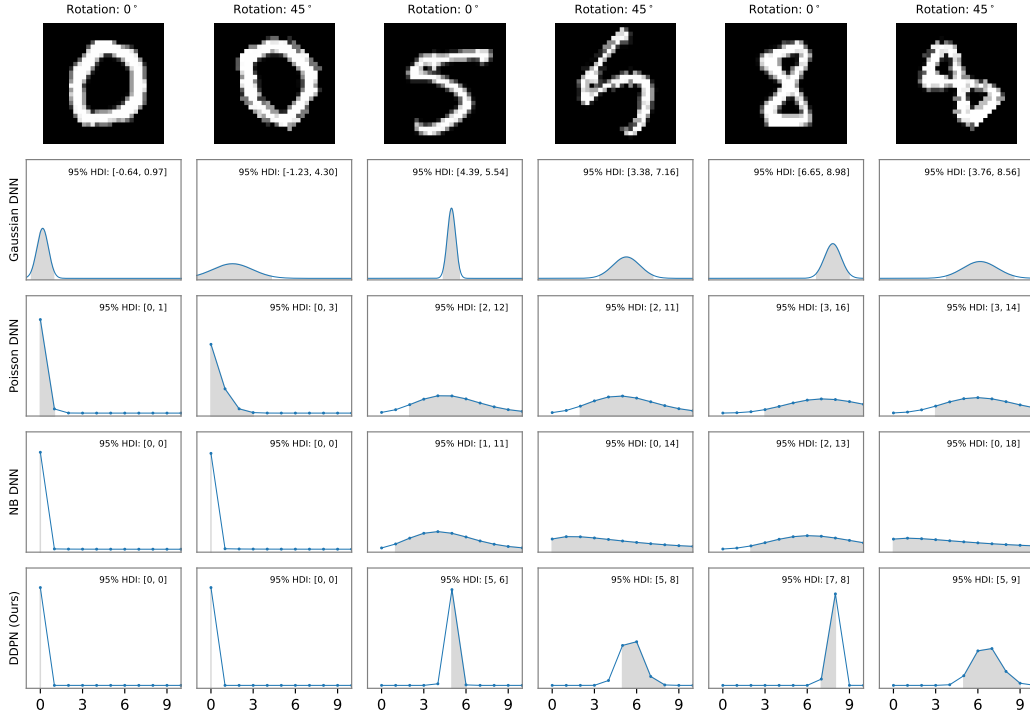


Figure 1: Columns: We show MNIST examples, along with out-of-distribution rotations. Rows: we show the predictive distributions, along with the 95% Highest Density Interval (HDI) of probabilistic neural nets trained with Gaussian, Poisson, Negative Binomial (NB) and Double Poisson (DDPN) loss. The Gaussian DNN row produces various pathologies: 1) non-zero probability mass for infeasible real values such as 8.13; 2) unbounded predictive intervals that cross 0 (i.e., the 0 digit HDI is  $[-0.64, 0.97]$ ); and 3) predictive intervals that fall between two discrete values (ie., the 5 digit in the third column has an HDI of  $[4.39, 5.54]$ ). The rows Poisson DNN and NB DNN demonstrate predictive distributions that are equi- and over-dispersed (respectively), resulting in a predictive variance that increases monotonically as the digits increase, regardless of input quality. Deep Double Poisson Networks (DDPN) resolve all of these issues.

[13, 14, 15, 16, 17, 18], the number of cars in a parking lot [19], traffic flow [20, 21, 22], agricultural yields [23], inventory of product on shelves [24], and bacteria in microscopic images [25]. In this paper, we are interested in training neural networks to output a flexible, calibrated, and properly specified predictive distribution over discrete counts.

Historically, uncertainty representation in regression tasks has been addressed by parameterizing the mean and variance of a Gaussian distribution as the outputs of a neural network,  $[\hat{\mu}_i, \hat{\sigma}_i^2]^T = \mathbf{f}_{\Theta}(\mathbf{x}_i)$  [26]. The model is then trained to minimize Gaussian negative log likelihood loss (NLL) via gradient-based optimization. This form of input-conditional predictive variance is known as *heteroscedastic regression*.

Recent work has improved the performance of heteroscedastic regression by mediating the influence of  $\hat{\sigma}^2$  on the gradient of the mean, which can cause instability during training, miscalibrated predictive variance, or a poor mean fit. Immer et al. [27] address these issues by reparameterizing the neural network to output the natural parameters of the Gaussian distribution. Seitzer et al. [28] propose a modified loss function and introduce a hyperparameter,  $\beta \in [0, 1]$ , which tempers the impact of  $\hat{\sigma}^2$  on the gradient of the mean. Stirn et al. [29] re-scale the gradient of  $\hat{\mu}$  and modify the architecture of the underlying network to include separate sub-networks for  $\hat{\mu}$  and  $\hat{\sigma}^2$ , along with the stop gradient operation to prevent the gradient of  $\hat{\sigma}^2$  from impacting the  $\hat{\mu}(\mathbf{x})$  sub-network.

However, when each of these methods is applied to count regression, the model is trained to output an input-dependent probability *density* function,  $p(y|\mathbf{f}_{\Theta}(\mathbf{x}))$ ;  $y \in \mathbb{R}$ , over a *discrete* output space, i.e.  $y \in \mathbb{Z}_{\geq 0}$ . This creates pathologies wherein the model outputs non-zero probability mass over

infeasible continuous values. Consider, for example, Figure 1. In each column an example from the MNIST dataset [30] is visualized, along with the same digit rotated to be out-of-distribution relative to the training data (models were trained without rotation-based data augmentation). The labels,  $y$ , can take any value in the set  $\{0, 1, 2, \dots, 9\}$ . Along the rows, we visualize predictive distributions of networks trained with different likelihood settings, along with their corresponding 95% Highest Density Interval (HDI). The Gaussian predictive distribution suffers from three issues. First, it assigns positive probability to regression targets outside the discrete label set, such as 7.9 or 8.1. Second, the predictive distribution is unbounded, and thus allows for negative values. In the first and second columns, the predictive HDI for the digit 0 crosses 0; count regression problems are restricted to the non-negative integers,  $\mathbb{Z}_{\geq 0}$ . Third, the bounds of the HDIs tend to fall in between two integers, limiting their usefulness. In the third column, the Gaussian network for the 5 digit has high confidence that the mean is near 5, but the HDI is  $[4.39, 5.54]$ . To overcome these limitations, we desire a properly specified probability *mass* function (conditional on the input features),  $p(y|\mathbf{f}_{\Theta}(\mathbf{x}))$ ;  $y \in \mathbb{Z}_{\geq 0}$ .

The most straightforward approach to learn a discrete predictive distribution is to train a network to minimize Poisson NLL. However, the Poisson parameterization of the neural network suffers from the *equi-dispersion* assumption: predictive mean and variance of the Poisson distribution are the same ( $\hat{\lambda} = \hat{\mu} = \hat{\sigma}^2$ ). Therefore, the model is not flexible enough to produce separate input-dependent mean and variance predictions. Another common alternative is to train the network to minimize Negative Binomial (NB) NLL. The Negative Binomial breaks *equi-dispersion* by introducing another parameter to the PMF. This helps disentangle the mean and variance, but suffers from the *over-dispersion* assumption:  $\hat{\sigma}^2 \geq \hat{\mu}$ . Consequently, this model is not flexible enough to assign uncertainty less than its mean prediction for a given input. In both rows two (Poisson DNN) and three (NB DNN) of Figure 1, the predictive variance grows monotonically as the digits increase, regardless of the noise in the corresponding input.

**Our Contributions** To address these issues, we introduce Deep Double Poisson Networks (DDPN). We train a neural network to output the parameters of the Double Poisson Distribution [31], a highly flexible probability mass function. We introduce a novel loss, the DDPN objective, for training DDPNs and propose a parameterization that is amenable to gradient-based training methods with neural networks. In contrast to Gaussian-based heteroscedastic regressors, DDPN outputs a properly specified PMF,  $p(y|\mathbf{f}_{\Theta}(\mathbf{x}))$ ;  $y \in \mathbb{Z}_{\geq 0}$ , while also maintaining high mean accuracy and probabilistic calibration. DDPN is flexible enough to handle over-, under- and equi-dispersion, making it a superior choice to the Poisson or Negative Binomial alternatives for discrete predictive uncertainty quantification. We show across a variety of data modalities (tabular, image, point cloud, and text) that DDPNs exhibit high accuracy and produce reliable aleatoric uncertainty representations, matching or exceeding the performance and calibration of Gaussian-based alternatives. Finally, we show that DDPN exhibits better out-of-distribution detection than existing techniques.

## 2 Predictive Uncertainty with Neural Networks

Predictive uncertainty can be decomposed into two types: *epistemic* (uncertainty of the model weights) and *aleatoric* uncertainty (observation noise) [2, 32].

### 2.1 Epistemic Uncertainty

Epistemic uncertainty refers to uncertainty due to model misspecification. Modern neural networks tend to be significantly underspecified by the data, which introduces a high degree of epistemic uncertainty [33]. In general, epistemic uncertainty can be reduced through additional data acquisition.

A variety of techniques have been proposed to explicitly represent epistemic uncertainty with neural networks. Given a dataset,  $\mathcal{D}$ , Bayesian inference seeks to learn the posterior distribution over a network’s parameters,  $p(\Theta|\mathcal{D})$  to explicitly quantify epistemic uncertainty [33]. Inference involves learning the posterior, which is performed through marginalization, or integration, over the parameter space. In practice, this integral is intractable and must be approximated with MCMC methods, most notably Hamiltonian Monte Carlo (HMC) [34, 35]. However, in the age of large-scale deep learning, even HMC is difficult to scale, and further approximations are required. Variational methods seek to approximate the posterior with a simpler, *variational* distribution (e.g., multivariate Gaussian), and minimize the KL-divergence between the posterior and variational distributions by maximizing

the Expected Lower Bound objective (ELBO). Laplace approximation first trains the network with SGD to find the maximum a posteriori (MAP) estimate. A second, post-hoc step is then performed to approximate the posterior with a multivariate Gaussian that is centered at the MAP, with covariance informed by the Hessian [36].

A simple and popular approach to estimate epistemic uncertainty is deep ensembles [1, 37]. This technique can be viewed as a Bayesian model average where the posterior is sampled at multiple local modes [38, 33]. Deep ensembles have a number of attractive properties: 1) they generally improve predictive performance [39]; 2) they can model more complex predictive distributions; and 3) they effectively represent uncertainty over learned weights, which leads to better probabilistic calibration.

## 2.2 Heteroscedastic Regression for Aleatoric Uncertainty

Aleatoric uncertainty quantifies observation noise and generally cannot be reduced with more data [32, 2]. In practice, this uncertainty can be introduced by low resolution sensors, blurry images, or intrinsic noise of a signal. Aleatoric noise is commonly modeled in machine learning by fitting the parameters of a distribution over the output. The model (i.e., neural network) has a single set of weights, but now predicts the parameters of an distribution over the target, rather than a point prediction.

To model aleatoric uncertainty in continuous regression, the common practice is to specify a neural network that outputs the mean and log variance of a Gaussian,  $[\hat{\mu}_i, \log \hat{\sigma}_i^2]^T = \mathbf{f}_{\Theta}(\mathbf{x}_i)$ , and train it to minimize Gaussian NLL loss [26, 2]. Recent work has identified instabilities in this training procedure and seeks to correct them through reparameterization and Laplace approximation [27], training separate mean and variance sub-networks [29], or re-scaling the gradients of the loss w.r.t the mean [28]. Similarly, one can specify a neural network that outputs the parameters of a discrete distribution for count regression. For example, Fallah et al. [40] train a neural network to predict the mean and variance parameter,  $\lambda$ , of a Poisson distribution, while Xie et al. [41] apply this idea to the Negative Binomial distribution. As discussed previously, these approaches suffer from the equi- and over-dispersion assumptions. Other options for flexible distribution fitting include the Double Poisson [31, 42], Conway-Maxwell-Poisson distribution [43, 44], Gamma-count, and Generalized Poisson [45, 42]. In contrast to these other flexible distribution functions, the Double Poisson is highly interpretable. Its two parameters,  $\mu$ , and  $\phi$ , represent the mean and inverse-dispersion [46], which can be easily translated into the variance,  $\sigma^2 \approx \frac{\mu}{\phi}$ . These properties make it attractive for use with neural networks as a predictive distribution.

## 2.3 Measuring Calibration

Recently, significant attention has been paid to measuring the quality of predictive uncertainty representations produced by neural networks, showing that they tend to be miscalibrated [47, 48]. Expected calibration error (ECE) was originally proposed to measure calibration for binary outputs [49], while [50] extended the metric to the multi-class case. More recently, a similar score (also termed the expected calibration error) was defined for regression models in [51]. Inspired by [52], the regression ECE quantifies calibration with an estimate of the distance between the probability integral transform (PIT) of the predicted CDF and  $\text{Uniform}[0, 1]$  (see [4] for a more detailed derivation). However, recent work has shown that this approach implicitly assumes continuity of the CDF, thus introducing bias when applied to discrete regression problems [53].

In this paper, we use negative log likelihood (NLL) to quantify calibration, as it is a standard measure of a probabilistic model’s quality and is a strictly proper scoring rule [54], meaning that it is uniquely minimized by a perfectly specified model. In an effort to identify models that are both *calibrated* and *useful* as suggested by [55], we also describe the *sharpness* of the predictive distribution by measuring the median precision (MP).

## 3 Deep Double Poisson Networks (DDPN)

In this section, we introduce the Deep Double Poisson Network (DDPN), which outputs the parameters of the Double Poisson distribution [31, 42]. The main idea of DDPN is to flexibly and accurately model an input-conditional predictive distribution over the space of discrete outputs (See Figure 1). To accomplish this, we propose a novel loss function (Equation 2) to train DDPNs.

We assume access to a dataset,  $\mathcal{D}$ , with  $N$  training examples  $\{\mathbf{x}_i, y_i\}_{i=1}^N$ , where each  $y_i \in \mathbb{Z}_{\geq 0}$  is drawn from some unknown nonnegative discrete distribution  $p(y_i|\mathbf{x}_i)$ . Let  $\mathcal{X}$  denote the space of all possible inputs  $\mathbf{x}$ , let  $\mathcal{P}$  denote the space of all possible distributions over  $\mathbb{Z}_{\geq 0}$ , and let  $\boldsymbol{\psi} \in \mathbb{R}^d$  denote a vector of parameters identifying a specific  $p \in \mathcal{P}$ . We wish to model this distribution via a neural network  $\mathbf{f}_{\Theta} : \mathcal{X} \rightarrow \mathcal{P}$  with learnable weights  $\Theta$ . In practice, we model  $\mathbf{f}_{\Theta} : \mathcal{X} \rightarrow \boldsymbol{\psi} \in \mathbb{R}^d$ . Given such a network, we obtain a predictive distribution,  $\hat{p}(y|\mathbf{f}_{\Theta}(\mathbf{x}))$ , for any input  $\mathbf{x}$ .

In particular, suppose that we restrict our output space to  $\mathcal{P}_{DDP} \subset \mathcal{P}$ , a family of Double Poisson distributions over  $y$ . Any distribution  $p \in \mathcal{P}_{DDP}$  is uniquely parameterized by  $\boldsymbol{\psi} = [\mu, \phi]^T \succ \mathbf{0}$ , with distribution function  $p : \mathbb{Z}_{\geq 0} \rightarrow [0, 1]$  defined as follows (where  $c$  is a normalizing constant):

$$p(y|\mu, \phi) = \frac{\phi^{\frac{1}{2}} e^{-\phi\mu}}{c(\mu, \phi)} \left( \frac{e^{-y} y^y}{y!} \right) \left( \frac{e\mu}{y} \right)^{\phi y}, \quad c(\mu, \phi) \approx 1 + \frac{1-\phi}{12\mu\phi} \left( 1 + \frac{1}{\mu\phi} \right) \quad (1)$$

### 3.1 DDPN Objective

Let  $Z$  denote a random variable with a Double Poisson distribution function (Equation 1). Then we say  $Z \sim \text{DP}(\mu, \phi)$ , with  $\mathbb{E}[Z] \approx \mu$  and  $\text{Var}[Z] \approx \frac{\mu}{\phi}$  [31]. To learn the weights  $\Theta$  of a neural network  $\mathbf{f}_{\Theta}$ , we output  $[\log \hat{\mu}_i, \log \hat{\phi}_i]^T = \mathbf{f}_{\Theta}(\mathbf{x}_i)$ <sup>1</sup> and minimize the Double Poisson NLL:

$$\mathcal{L}_{DDPN}(y_i, \hat{\mu}_i, \hat{\phi}_i) = \frac{1}{N} \sum_{i=1}^N \left( -\frac{1}{2} \log \hat{\phi}_i + \hat{\phi}_i \hat{\mu}_i - \hat{\phi}_i y_i (1 + \log \hat{\mu}_i - \log y_i) \right) \quad (2)$$

During training, we minimize  $\mathcal{L}_{DDPN}$  iteratively via stochastic gradient descent (or common variants). We provide a full derivation of Equation 2 in Appendix A.2.

### 3.2 $\beta$ -DDPN: NLL Loss Modifications

As first noted in [28], when training a heteroscedastic regressor with Gaussian likelihood, the ability of a neural network to fit the mean can be harmed by the presence of the predicted variance term in the partial derivative of the mean. We observe that this same phenomenon exists with DDPN. We have the following partial derivatives with respect to  $\hat{\mu}$  and  $\hat{\phi}$ :

$$\frac{\partial \mathcal{L}_{DDPN}}{\partial \hat{\mu}_i} = \hat{\phi}_i \left( 1 - \frac{y_i}{\hat{\mu}_i} \right), \quad \frac{\partial \mathcal{L}_{DDPN}}{\partial \hat{\phi}_i} = -\frac{1}{2\hat{\phi}_i} + \hat{\mu}_i - y_i (1 + \log \hat{\mu}_i - \log y_i) \quad (3)$$

Notice that if  $\hat{\phi}_i$  is sufficiently small (corresponding to large variance), it can completely zero out  $\frac{\partial \mathcal{L}_{DDPN}}{\partial \hat{\mu}_i}$  regardless of the current value of  $\hat{\mu}_i$ . Thus, during training, a neural network can converge to (and get “stuck” in) suboptimal solutions wherein poor mean fit is explained away via large uncertainty values. To remedy this behavior, we propose a modified loss function, the  $\beta$ -DDPN:

$$\mathcal{L}_{\beta-DDPN}(y_i, \hat{\mu}_i, \hat{\phi}_i) = \frac{1}{N} \sum_{i=1}^N \left[ \hat{\phi}_i^{-\beta} \right] \left( -\frac{1}{2} \log \hat{\phi}_i + \hat{\phi}_i \hat{\mu}_i - \hat{\phi}_i y_i (1 + \log \hat{\mu}_i - \log y_i) \right) \quad (4)$$

where  $[\cdot]$  denotes the *stop-gradient* operation. With this modification we can effectively temper the effect of large variance on mean fit. We now have the following partial derivatives:

$$\frac{\partial \mathcal{L}_{\beta-DDPN}}{\partial \hat{\mu}_i} = \left( \hat{\phi}_i^{1-\beta} \right) \left( 1 - \frac{y_i}{\hat{\mu}_i} \right), \quad \frac{\partial \mathcal{L}_{\beta-DDPN}}{\partial \hat{\phi}_i} = -\frac{1}{2\hat{\phi}_i^{1+\beta}} + \hat{\mu}_i - y_i (1 + \log \hat{\mu}_i - \log y_i) \quad (5)$$

<sup>1</sup>The network,  $\mathbf{f}_{\Theta}$ , outputs the parameters,  $\hat{\mu}$ , and  $\hat{\phi}$ , on a log scale to ensure positivity and encourage numerical stability during training. We simply exponentiate whenever  $\hat{\mu}_i$  or  $\hat{\phi}_i$  are needed (i.e., to evaluate the density function in Equation 1)

The Double Poisson  $\beta$ -NLL is parameterized by  $\beta \in [0, 1]$ , where  $\beta = 0$  recovers the original Double Poisson NLL and  $\beta = 1$  corresponds to fitting the mean,  $\mu$ , with no respect to  $\phi$  (while still performing normal weight updates to fit the value of  $\phi$ ). Thus, we can consider the value of  $\beta$  as providing a smooth interpolation between NLL and a more mean-focused loss.

### 3.3 DDPN Ensembles

The formulation of DDPN described above applies to neural networks with a single forward pass. As noted in Section 2, multiple independently trained neural networks can be combined to improve mean fit and distributional calibration by modeling epistemic uncertainty. Thus, we propose a technique for constructing an ensemble of DDPNs to further enhance the quality of the predictive distribution. Following [1, 38], we train  $M$  different DDPNs on the *same* dataset and only vary the random initialization point. This produces  $M$  different solutions  $\{\Theta_m\}_{m=1}^M$  yielding  $M$  distinct predictive distributions for any given input,  $\{p(y_i|\mathbf{f}_{\Theta_m}(\mathbf{x}_i))\}_{m=1}^M$ . For our ensemble prediction, we form a uniform mixture of each distribution:  $p(y_i|\mathbf{x}_i) = \frac{1}{M} \sum_{m=1}^M p(y_i|\mathbf{f}_{\Theta_m}(\mathbf{x}_i))$ . In Appendix A.3 we provide well-known equations for recovering the mean and variance of this mixture distribution [56, 57].

## 4 Experiments

We evaluate DDPN across a variety of count regression tasks based on tabular, image, point cloud, and text data. We compare a number of baselines, including a Poisson Generalized Linear Model (GLM), a Negative Binomial GLM, a Gaussian Deep Neural Network (DNN) [26], a Poisson DNN [40], Negative Binomial DNN [41], the ‘‘faithful’’ DNN regressor presented in Stirn et al. [29], the naturally parametrized Gaussian regressor from Immer et al. [27], and the reparameterized network (with  $\beta = 1$ ) from Seitzer et al. [28]. Additionally, we show the impact of the  $\beta$ -DDPN modification presented in Section 3.2. We refer to these as ‘‘single forward pass’’ methods. We also ensemble our method and compare to ensembles of Gaussian, Poisson, and Negative Binomial DNNs to demonstrate the impact of modeling both aleatoric and epistemic uncertainty. Gaussian ensembles are formed using the technique introduced in [1], while Poisson and Negative Binomial ensembles follow the same prediction strategy outlined in Section 3.3. All experiments are implemented in PyTorch [58]. Choices related to network architecture, hardware and hyperparameter selection are reported in Appendix B. Source code is freely available online<sup>2</sup>.

Each regression method is evaluated in terms of three criteria. First, Mean Absolute Error (MAE) measures the predictive accuracy and mean fit; lower values imply higher accuracy. Second, Negative Log Likelihood (NLL) measures the quality of the predictive distribution [59]; lower values imply greater agreement between the predictive distribution  $p$  and the observed label  $y_i$ . To facilitate comparison between NLL obtained from continuous and discrete models, we use the continuity correction to convert Gaussian densities into probabilities. Given a predicted Gaussian CDF  $\hat{F}_i$  for some input-output pair  $(x_i, y_i)$ , we take  $P(Y = y_i|\hat{F}_i) \approx \hat{F}_i(y_i + \frac{1}{2}) - \hat{F}_i(y_i - \frac{1}{2})$ . We then compute NLL as the average of  $-\log P(Y = y_i|\hat{F}_i)$  across the evaluation set. Finally, we report Median Precision (MP), which is calculated as the median of the precision values,  $\lambda_i = \frac{1}{\sigma_i^2}$ , across the evaluation set. This metric measures the sharpness of the predictive distribution; higher values correspond to more concentrated probability mass. For each technique, we train and evaluate 5 models and report the empirical mean and standard deviation (in parentheses). To form ensembles, these same 5 models were combined.

### 4.1 Simulation Experiment

To clearly illustrate the flexibility of the DDPN in modeling count data, we simulate a dataset that exhibits both under-dispersion (variance lower than the count) and over-dispersion (variance higher than the count). The exact data generating process is described in Appendix B.1. We train a small multi-layer perceptron (MLP) to output the parameters of a Gaussian, Poisson, Negative Binomial, or Double Poisson distribution using the appropriate NLL loss. The resultant models<sup>2</sup>

<sup>2</sup><https://anonymous.4open.science/r/ddpn-651F/README.md>

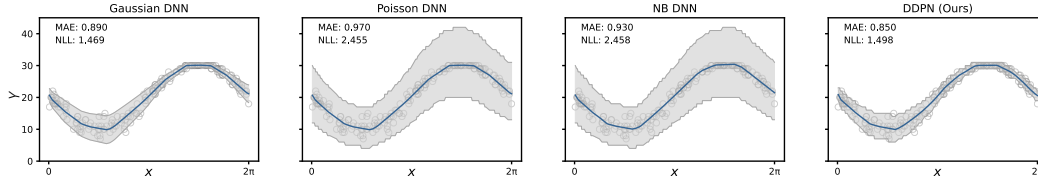


Figure 2: Simulation experiment with heteroscedastic variance over discrete outputs. Here we model the case of both under-dispersion (on the high values of  $y$ ) and over-dispersion (on the low values of  $y$ ). We visualize the mean fit and predictive uncertainty (centered 95% credible interval) of each of 4 probabilistic neural networks on the test split of the dataset, along with the mean absolute error (MAE) and NLL. All models adequately fit the mean. However, only the Gaussian DNN and DDPN correctly recover the heteroscedastic pattern in both under- and over-dispersed regions, while the Poisson DNN and NB DNN lack sufficient flexibility to capture under-dispersion.

		Bikes			Collision		
		MAE ( $\downarrow$ )	NLL ( $\downarrow$ )	MP ( $\times 10^{-3}$ , $\uparrow$ )	MAE ( $\downarrow$ )	NLL ( $\downarrow$ )	MP ( $\uparrow$ )
Single Forward Pass	Poisson GLM	110.07 (2.59)	9.81 (0.02)	8.83 (0.34)	0.394 (0.00)	1.186 (0.01)	0.814 (0.01)
	NB GLM	190.03 (0.00)	10.83 (0.09)	<b>749</b> (265)	0.322 (0.02)	1.120 (0.01)	0.729 (0.07)
	Gaussian DNN	38.70 (2.65)	5.00 (0.04)	0.55 (0.09)	0.305 (0.00)	0.772 (0.10)	5.424 (1.69)
	Poisson DNN	<b>27.76</b> (0.34)	5.81 (0.04)	<u>6.98</u> (0.08)	0.316 (0.01)	1.181 (0.00)	0.871 (0.00)
	NB DNN	32.33 (6.71)	4.72 (0.08)	1.23 (0.28)	0.277 (0.00)	1.183 (0.01)	0.802 (0.04)
	Stirn [29]	28.54 (0.40)	5.07 (0.06)	2.13 (0.04)	0.302 (0.00)	1.005 (0.00)	1.789 (0.06)
	Seitzer [28]	30.11 (0.87)	4.85 (0.04)	0.96 (0.13)	<u>0.274</u> (0.00)	0.731 (0.00)	6.440 (0.36)
	Immer [27]	35.30 (0.74)	5.03 (0.04)	0.56 (0.03)	<u>0.304</u> (0.00)	0.723 (0.00)	6.759 (0.45)
	DDPN (ours)	<u>28.18</u> (0.34)	<b>4.67</b> (0.01)	1.39 (0.07)	0.280 (0.00)	<u>0.719</u> (0.01)	<u>7.746</u> (2.30)
	$\beta$ -DDPN (ours)	28.93 (0.80)	<u>4.70</u> (0.01)	1.14 (0.14)	<b>0.269</b> (0.00)	<b>0.707</b> (0.01)	<b>8.343</b> (0.90)
Deep Ensembles	Gaussian DNN [1]	34.40	4.87	0.44	0.282	0.756	4.323
	Poisson DNN	<u>26.01</u>	5.15	<b>3.97</b>	0.278	1.178	0.863
	NB DNN	28.00	4.62	0.93	<u>0.270</u>	1.179	0.799
	DDPN (ours)	<b>25.96</b>	<b>4.57</b>	<u>1.15</u>	0.271	<b>0.610</b>	8.567
	$\beta$ -DDPN (ours)	26.37	<u>4.60</u>	0.92	<b>0.270</b>	<u>0.697</u>	<b>18.228</b>

Table 1: Results on tabular datasets: We report the Mean Absolute Error (MAE), Negative Log Likelihood (NLL), and Median Precision (MP) for each method. We denote the best performer in **bold** and the second-best performer with an underline.

predictive distributions over the test split of the synthetic dataset are visualized in Figure 2. MAE and NLL are both reported in each panel of the figure.

DDPN clearly meets or exceeds the flexibility and accuracy of the Gaussian while maintaining a proper distribution over discrete counts. It achieves slightly better mean fit (lower MAE) and roughly equivalent calibration (NLL). Conversely, the Poisson and Negative Binomial DNNs are not flexible enough to recover the heteroscedastic variance pattern of the data.

## 4.2 Tabular Datasets

We perform two experiments on tabular datasets, one with high frequency counts, and one with low frequency counts. The Bikes dataset [60] describes the number of hourly bike rentals between the years 2011 and 2012 in the Capital bikeshare system. The features are the corresponding weather and seasonal information. The 25th, 50th, and 75th percentiles of the labels,  $y_i$ , are (40, 142, 281), indicating high frequency events. The Collisions dataset [61] is formed from the casualties, collisions, and vehicles tables in the United Kingdom’s 2022 Road Safety data. In this task, the goal is to predict the number of casualties in a collision, given features about the accident (i.e., drivers, vehicles, location, etc.). The labels are severely right-skewed, ranging from 1 to 16 with a mean of 1.278 and a median of 1. For each dataset, we train an MLP to output the parameters of each benchmarked distribution. See Table 1 for results.

In Bikes we observe DDPN surpasses state-of-art heteroscedastic Gaussian regression baselines in terms of mean fit and approaches the performance of the Poisson DNN. We note that Poisson likely performs well because the provided features are not sufficient for concentrated predictions and the data are naturally over-dispersed. On the other hand, both DDPN and  $\beta$ -DDPN outperform all methods in terms of calibration (NLL). Interestingly, the linear NB model has very high median precision (MP), but very poor NLL, indicating that its predictive distribution is over-confident and

		COCO-People (Image)			Inventory (Point Cloud)		
		MAE ( $\downarrow$ )	NLL ( $\downarrow$ )	MP ( $\uparrow$ )	MAE ( $\downarrow$ )	NLL ( $\downarrow$ )	MP ( $\uparrow$ )
Single Forward Pass	Gaussian DNN	2.010 (0.03)	2.308 (0.02)	0.371 (0.04)	0.904 (0.01)	1.559 (0.01)	0.704 (0.05)
	Poisson DNN	2.013 (0.14)	2.393 (0.08)	0.388 (0.04)	0.960 (0.02)	1.763 (0.00)	0.252 (0.00)
	NB DNN	2.082 (0.30)	2.284 (0.04)	0.283 (0.15)	0.965 (0.01)	1.801 (0.03)	0.235 (0.03)
	Stirn et al. [29]	2.045 (0.20)	2.490 (0.08)	0.312 (0.08)	0.927 (0.03)	1.651 (0.02)	<b>1.073</b> (0.13)
	Seitzer et al. [28]	<u>2.003</u> (0.11)	2.470 (0.07)	<u>0.432</u> (0.16)	<b>0.888</b> (0.01)	<b>1.545</b> (0.01)	0.786 (0.04)
	Immer et al. [27]	2.129 (0.26)	2.359 (0.09)	0.292 (0.13)	0.925 (0.02)	1.587 (0.02)	<u>0.700</u> (0.02)
	DDPN (ours)	2.148 (0.23)	<b>2.251</b> (0.06)	0.366 (0.24)	<u>0.900</u> (0.01)	<u>1.555</u> (0.01)	0.697 (0.04)
	$\beta$ -DDPN (ours)	<b>1.962</b> (0.35)	2.517 (0.15)	<b>0.785</b> (0.37)	0.900 (0.01)	1.560 (0.02)	0.745 (0.03)
Deep Ensembles	Gaussian DNN [1]	1.941	2.195	0.274	0.873	1.511	<u>0.643</u>
	Poisson DNN	1.875	2.141	<u>0.278</u>	0.924	1.754	0.244
	NB DNN	<u>1.849</u>	2.073	0.124	0.902	1.790	0.225
	DDPN (ours)	1.904	<u>1.962</u>	0.194	<u>0.861</u>	<u>1.500</u>	0.641
	$\beta$ -DDPN (ours)	<b>1.701</b>	<b>1.891</b>	<b>0.296</b>	<b>0.851</b>	<b>1.486</b>	<b>0.664</b>

Table 2: Results on vision datasets. We denote the best performer in **bold** and the second-best performer with an underline.

is not truly calibrated. Both DDPN and  $\beta$ -DDPN appropriately balance calibration and sharpness. Additionally, modeling epistemic uncertainty via ensembling provides significant improvements in mean fit and calibration, relative to benchmarks. In *Collisions*, we see that  $\beta$ -DDPN outperforms all baselines in terms of mean fit, calibration, and sharpness. DDPN also performs well on these three dimensions and is competitive with Seitzer in terms of mean fit. Overall, these results suggest that DDPN is effective for both high and low-frequency counts. It is especially useful for fitting low-frequency predictive distributions, as it is able to concentrate well-calibrated probability mass around the ground truth value.

### 4.3 Vision Datasets

We introduce an image regression task on the person class of MS-COCO [62], which we call *COCO-People*. In this dataset, the task is to predict the number of people in each image. Additionally, we define an inventory counting task [24], where the goal is to predict the number of objects on a retail shelf from an input point cloud (see Figure 15 in the Appendix for an example). For *COCO-People*, each model was trained with a small MLP on top of the pooled output from a ViT backbone (initialized from the *vit-base-patch16-224-in21k* checkpoint [63, 64]). For the *Inventory* dataset, each model was fitted with a variant of CountNet3D [24] that was modified to output the parameters of a distribution instead of regressing the mean directly. See Table 2 for results.

In *COCO-People* we see strong performance in terms of both mean fit (MAE) and calibration (NLL), with either DDPN or  $\beta$ -DDPN outperforming all methods. As expected, DDPN outperforms benchmarks in terms of calibration, while  $\beta$ -DDPN yields the sharpest predictive distributions and best mean performance. We show example predictions from the *COCO-People* test set in Appendix C.1. In *Inventory*, Seitzer et al. achieves the best results in performance and calibration. However, DDPN achieves nearly identical calibration and competitive MAE performance. In both datasets, the ensembled  $\beta$ -DDPN results in the best mean fit, calibration, and sharpest predictive distributions.

### 4.4 Language Dataset

Finally, we predict user ratings from the “Patio, Lawn, and Garden” split of a collection of Amazon reviews [65]. The objective in this task is to predict the value of a review (1-5 stars) from an input text sequence. All text regression models were constructed as a small MLP on top of the [CLS] token in the output layer of a DistilBert backbone (starting from the *distilbert-base-cased*

		Amazon Reviews		
		MAE ( $\downarrow$ )	NLL ( $\downarrow$ )	MP ( $\uparrow$ )
Single Forward Pass	Gaussian DNN	0.326 (0.01)	0.834 (0.09)	7.753 (1.50)
	Poisson DNN	0.609 (0.04)	1.705 (0.00)	0.205 (0.00)
	NB DNN	0.746 (0.09)	1.711 (0.00)	0.205 (0.00)
	Stirn et al. [29]	<b>0.301</b> (0.00)	0.878 (0.02)	<b>8.789</b> (0.61)
	Seitzer et al. [28]	0.306 (0.01)	0.786 (0.04)	8.308 (0.97)
	Immer et al. [27]	0.310 (0.00)	<b>0.728</b> (0.01)	6.671 (1.1)
	DDPN (ours)	0.311 (0.00)	0.800 (0.01)	5.553 (0.30)
	$\beta$ -DDPN (ours)	<u>0.302</u> (0.00)	1.027 (0.15)	<u>8.515</u> (1.48)
Deep Ensembles	Gaussian DNN [1]	0.306	<b>0.726</b>	6.515
	Poisson DNN	0.600	1.702	0.205
	NB DNN	0.750	1.707	0.205
	DDPN (ours)	<u>0.295</u>	<u>0.729</u>	<u>6.632</u>
	$\beta$ -DDPN (ours)	<b>0.281</b>	0.753	<b>11.30</b>

Table 3: Results on a natural language dataset.



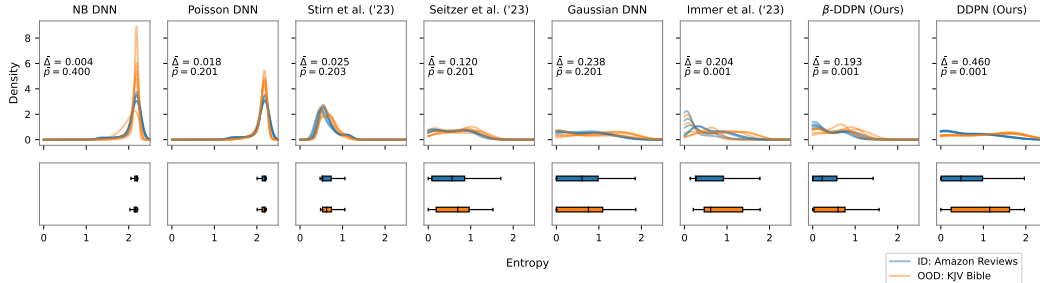


Figure 3: In-distribution (ID) vs. out-of-distribution (OOD) behavior for regression models trained on Amazon Reviews. We train each method five times, and plot the KDE-smoothed empirical distributions of entropy values obtained from the ID (Amazon Reviews) and OOD (KJV Bible) datasets. Additionally, we provide a box plot with an IQR of aggregated entropy values. We perform a two-sample permutation test with the difference-of-means statistic ( $\Delta$ ) and display, on the corresponding KDE plot, the average statistic ( $\hat{\Delta}$ ) across all models, along with the average p-value ( $\hat{p}$ ). A larger  $\hat{\Delta}$  is desirable, as it corresponds to a greater amount of entropy on OOD than ID inputs. Our DDPN model shows the greatest ability to distinguish between ID and OOD inputs.

checkpoint) [66]. See Table 3 for re-  
results.

Here we observe that  $\beta$ -DDPN performs favorably in terms of mean fit, essentially matching the predictive performance of Stirn. Seitzer and Immer both yield the best results in terms of calibration, while Stirn and  $\beta$ -DDPN produce the sharpest distributions. These results suggest that both Stirn and  $\beta$ -DDPN output sharp point masses around the true value, while Seitzer and Immer output more diffuse, conservative predictive distributions. We again note the positive impact of ensembling DDPN as this generally improves the quality of the predictive distribution.

#### 4.5 Out-of-Distribution Behavior

In this section, we compare the out-of-distribution (OOD) behavior of DDPNs to existing methods. To assess OOD behavior, for each model that has been trained on Amazon Reviews, we feed it verses from the King James Version of the Holy Bible [67, 68], and compute the entropy [69] of each of the resultant predictive distributions; we call these OOD entropy values. We do the same with the test split of Amazon Reviews, and call them in-distribution (ID) entropy values. We then compare the empirical distributions of these entropy values [5] by performing a one-sided permutation test [70] on the difference of means. This procedure outputs a test statistic,  $\Delta = \bar{x}_{OOD} - \bar{x}_{ID}$ , and a p-value (for more details see Appendix B.7). Higher entropy indicates higher uncertainty in a model’s predictive distributions. Thus, we expect that the models most able to distinguish between ID / OOD will have the larger  $\Delta$  since their mean entropy should be higher for OOD inputs than ID inputs.

The results of our experiment are displayed in Figure 3. With statistical significance, DDPN shows the greatest ability of all benchmarked regression models to differentiate between ID and OOD inputs, as demonstrated by the largest  $\hat{\Delta}$  (the average  $\Delta$  across trials). Existing count regression techniques (NB DNN, Poisson DNN) fail to exhibit any separation between predictive entropy on ID and OOD data. We note that of all Gaussian regression approaches, only [27] achieves a significant gap between ID and OOD entropies. For a similar analysis showing the supremacy of DDPN *ensemble* methods in terms of OOD behavior, see Appendix B.7. Additionally, we provide a case study of OOD detection in Appendix C.2. In particular, Figure 7 highlights the effective OOD behavior of DDPN.

In Section 3.2 we discussed the motivation for  $\beta$ -DDPN as a mechanism to tune the prioritization of mean accuracy and calibration. Empirically, this hypothesis is generally supported by our experiments. The  $\beta$  modification used to enhance mean fit appears to hurt a model’s recognition of OOD. From all experiments our general conclusion is the virtue of  $\beta$ -DDPN is highly accurate mean prediction, and concentrated predictive intervals, while the advantage of standard DDPN is reliable calibration and effective OOD detection.

## 5 Conclusion

Overall, we conclude that DDPNs are well-suited for complicated count regression tasks. Our main findings are that DDPNs 1) vastly outperform existing deep learning methods with discrete predictive distributions; 2) match or exceed the performance of state-of-the-art heteroscedastic regression techniques; 3) address pathologies with Gaussian-based heteroscedastic regressors applied to discrete counts; and 4) provide superior out-of-distribution detection, compared to existing methods. Moreover, DDPNs are general and can be applied to a variety of tasks and data modalities.

## References

- [1] B. Lakshminarayanan, A. Pritzel, and C. Blundell, “Simple and scalable predictive uncertainty estimation using deep ensembles,” *Advances in neural information processing systems*, vol. 30, 2017.
- [2] A. Kendall and Y. Gal, “What uncertainties do we need in bayesian deep learning for computer vision?” *Advances in neural information processing systems*, vol. 30, 2017.
- [3] J. Gawlikowski, C. R. N. Tassi, M. Ali, J. Lee, M. Humt, J. Feng, A. Kruspe, R. Triebel, P. Jung, R. Roscher *et al.*, “A survey of uncertainty in deep neural networks,” *Artificial Intelligence Review*, vol. 56, no. Suppl 1, pp. 1513–1589, 2023.
- [4] V. Dheur and S. B. Taieb, “A large-scale study of probabilistic calibration in neural network regression,” in *International Conference on Machine Learning*. PMLR, 2023, pp. 7813–7836.
- [5] A. Amini, W. Schwarting, A. Soleimany, and D. Rus, “Deep evidential regression,” *Advances in neural information processing systems*, vol. 33, pp. 14 927–14 937, 2020.
- [6] W. Liu, X. Wang, J. Owens, and Y. Li, “Energy-based out-of-distribution detection,” *Advances in neural information processing systems*, vol. 33, pp. 21 464–21 475, 2020.
- [7] K. Kang, A. Setlur, C. Tomlin, and S. Levine, “Deep neural networks tend to extrapolate predictably,” *arXiv preprint arXiv:2310.00873*, 2023.
- [8] B. Settles, “Active learning literature survey,” 2009.
- [9] M. Ziatdinov, “Active learning with fully bayesian neural networks for discontinuous and nonstationary data,” *arXiv preprint arXiv:2405.09817*, 2024.
- [10] T. Yu, G. Thomas, L. Yu, S. Ermon, J. Y. Zou, S. Levine, C. Finn, and T. Ma, “Mopo: Model-based offline policy optimization,” *Advances in Neural Information Processing Systems*, vol. 33, pp. 14 129–14 142, 2020.
- [11] P. Jenkins, H. Wei, J. S. Jenkins, and Z. Li, “Bayesian model-based offline reinforcement learning for product allocation,” in *Proceedings of the AAAI Conference on Artificial Intelligence*, vol. 36, no. 11, 2022, pp. 12 531–12 537.
- [12] M. Abdar, F. Pourpanah, S. Hussain, D. Rezazadegan, L. Liu, M. Ghavamzadeh, P. Fieguth, X. Cao, A. Khosravi, U. R. Acharya *et al.*, “A review of uncertainty quantification in deep learning: Techniques, applications and challenges,” *Information fusion*, vol. 76, pp. 243–297, 2021.
- [13] Y. Zhang, D. Zhou, S. Chen, S. Gao, and Y. Ma, “Single-image crowd counting via multi-column convolutional neural network,” in *Proceedings of the IEEE conference on computer vision and pattern recognition*, 2016, pp. 589–597.
- [14] D. Lian, J. Li, J. Zheng, W. Luo, and S. Gao, “Density map regression guided detection network for rgb-d crowd counting and localization,” in *Proceedings of the IEEE/CVF Conference on Computer Vision and Pattern Recognition*, 2019, pp. 1821–1830.
- [15] Q. Zhang and A. B. Chan, “3d crowd counting via multi-view fusion with 3d gaussian kernels,” in *Proceedings of the AAAI conference on artificial intelligence*, vol. 34, no. 07, 2020, pp. 12 837–12 844.
- [16] Z. Zou, H. Shao, X. Qu, W. Wei, and P. Zhou, “Enhanced 3d convolutional networks for crowd counting,” *arXiv preprint arXiv:1908.04121*, 2019.
- [17] A. Luo, F. Yang, X. Li, D. Nie, Z. Jiao, S. Zhou, and H. Cheng, “Hybrid graph neural networks for crowd counting,” in *Proceedings of the AAAI conference on artificial intelligence*, vol. 34, no. 07, 2020, pp. 11 693–11 700.
- [18] W. Lin and A. B. Chan, “Optimal transport minimization: Crowd localization on density maps for semi-supervised counting,” in *Proceedings of the IEEE/CVF Conference on Computer Vision and Pattern Recognition*, 2023, pp. 21 663–21 673.
- [19] M.-R. Hsieh, Y.-L. Lin, and W. H. Hsu, “Drone-based object counting by spatially regularized regional proposal network,” in *Proceedings of the IEEE international conference on computer vision*, 2017, pp. 4145–4153.

- [20] Y. Lv, Y. Duan, W. Kang, Z. Li, and F.-Y. Wang, “Traffic flow prediction with big data: A deep learning approach,” *Ieee transactions on intelligent transportation systems*, vol. 16, no. 2, pp. 865–873, 2014.
- [21] C. Liu, D. Q. Huynh, Y. Sun, M. Reynolds, and S. Atkinson, “A vision-based pipeline for vehicle counting, speed estimation, and classification,” *IEEE Transactions on Intelligent Transportation Systems*, vol. 22, no. 12, pp. 7547–7560, 2021.
- [22] S. Li, F. Chang, C. Liu, and N. Li, “Vehicle counting and traffic flow parameter estimation for dense traffic scenes,” *IET Intelligent Transport Systems*, vol. 14, no. 12, pp. 1517–1523, 2020.
- [23] J. You, X. Li, M. Low, D. Lobell, and S. Ermon, “Deep gaussian process for crop yield prediction based on remote sensing data,” in *Proceedings of the AAAI conference on artificial intelligence*, vol. 31, no. 1, 2017.
- [24] P. Jenkins, K. Armstrong, S. Nelson, S. Gotad, J. S. Jenkins, W. Wilkey, and T. Watts, “Countnet3d: A 3d computer vision approach to infer counts of occluded objects,” in *Proceedings of the IEEE/CVF Winter Conference on Applications of Computer Vision*, 2023, pp. 3008–3017.
- [25] M. Marsden, K. McGuinness, S. Little, C. E. Keogh, and N. E. O’Connor, “People, penguins and petri dishes: Adapting object counting models to new visual domains and object types without forgetting,” in *Proceedings of the IEEE conference on computer vision and pattern recognition*, 2018, pp. 8070–8079.
- [26] D. A. Nix and A. S. Weigend, “Estimating the mean and variance of the target probability distribution,” in *Proceedings of 1994 IEEE international conference on neural networks (ICNN’94)*, vol. 1. IEEE, 1994, pp. 55–60.
- [27] A. Immer, E. Palumbo, A. Marx, and J. Vogt, “Effective bayesian heteroscedastic regression with deep neural networks,” *Advances in Neural Information Processing Systems*, vol. 36, 2024.
- [28] M. Seitzer, A. Tavakoli, D. Antic, and G. Martius, “On the pitfalls of heteroscedastic uncertainty estimation with probabilistic neural networks,” *arXiv preprint arXiv:2203.09168*, 2022.
- [29] A. Stirn, H. Wessels, M. Schertzer, L. Pereira, N. Sanjana, and D. Knowles, “Faithful heteroscedastic regression with neural networks,” in *International Conference on Artificial Intelligence and Statistics*. PMLR, 2023, pp. 5593–5613.
- [30] Y. LeCun, L. Bottou, Y. Bengio, and P. Haffner, “Gradient-based learning applied to document recognition,” *Proceedings of the IEEE*, vol. 86, no. 11, pp. 2278–2324, 1998.
- [31] B. Efron, “Double exponential families and their use in generalized linear regression,” *Journal of the American Statistical Association*, vol. 81, no. 395, pp. 709–721, 1986.
- [32] A. Der Kiureghian and O. Ditlevsen, “Aleatory or epistemic? does it matter?” *Structural safety*, vol. 31, no. 2, pp. 105–112, 2009.
- [33] A. G. Wilson and P. Izmailov, “Bayesian deep learning and a probabilistic perspective of generalization,” *Advances in neural information processing systems*, vol. 33, pp. 4697–4708, 2020.
- [34] T. Chen, E. Fox, and C. Guestrin, “Stochastic gradient hamiltonian monte carlo,” in *Proceedings of the 31st International Conference on Machine Learning*, ser. Proceedings of Machine Learning Research, E. P. Xing and T. Jebara, Eds., vol. 32, no. 2. Beijing, China: PMLR, 22–24 Jun 2014, pp. 1683–1691. [Online]. Available: <https://proceedings.mlr.press/v32/cheni14.html>
- [35] M. D. Hoffman, A. Gelman *et al.*, “The no-u-turn sampler: adaptively setting path lengths in hamiltonian monte carlo.” *J. Mach. Learn. Res.*, vol. 15, no. 1, pp. 1593–1623, 2014.
- [36] E. Daxberger, A. Kristiadi, A. Immer, R. Eschenhagen, M. Bauer, and P. Hennig, “Laplace redux-effortless bayesian deep learning,” *Advances in Neural Information Processing Systems*, vol. 34, pp. 20089–20103, 2021.
- [37] F. D’Angelo and V. Fortuin, “Repulsive deep ensembles are bayesian,” *Advances in Neural Information Processing Systems*, vol. 34, pp. 3451–3465, 2021.
- [38] S. Fort, H. Hu, and B. Lakshminarayanan, “Deep ensembles: A loss landscape perspective,” *arXiv preprint arXiv:1912.02757*, 2019.
- [39] T. G. Dietterich, “Ensemble methods in machine learning,” in *International workshop on multiple classifier systems*. Springer, 2000, pp. 1–15.

- [40] N. Fallah, H. Gu, K. Mohammad, S. A. Seyyedsalehi, K. Nourijelyani, and M. R. Eshraghian, “Nonlinear poisson regression using neural networks: A simulation study,” *Neural Computing and Applications*, vol. 18, pp. 939–943, 2009.
- [41] S.-M. Xie, “A neural network extension for solving the pareto/negative binomial distribution model,” *International Journal of Market Research*, vol. 64, no. 3, pp. 420–439, 2022.
- [42] D. Toledo, C. A. Umetsu, A. F. M. Camargo, and I. A. R. de Lara, “Flexible models for non-equidispersed count data: comparative performance of parametric models to deal with underdispersion,” *AStA Advances in Statistical Analysis*, vol. 106, no. 3, pp. 473–497, 2022.
- [43] G. Shmueli, T. P. Minka, J. B. Kadane, S. Borle, and P. Boatwright, “A useful distribution for fitting discrete data: revival of the conway–maxwell–poisson distribution,” *Journal of the Royal Statistical Society Series C: Applied Statistics*, vol. 54, no. 1, pp. 127–142, 2005.
- [44] A. Huang, “Mean-parametrized conway–maxwell–poisson regression models for dispersed counts,” *Statistical Modelling*, vol. 17, no. 6, pp. 359–380, 2017.
- [45] P. Consul and F. Famoye, “Generalized poisson regression model,” *Communications in Statistics-Theory and Methods*, vol. 21, no. 1, pp. 89–109, 1992.
- [46] J. E. Pustejovsky, “Implementing efron’s double poisson distribution in stan,” <https://www.jepusto.com/double-poisson-in-stan/>, September 2023, blog.
- [47] C. Guo, G. Pleiss, Y. Sun, and K. Q. Weinberger, “On calibration of modern neural networks,” in *International conference on machine learning*. PMLR, 2017, pp. 1321–1330.
- [48] M. Minderer, J. Djolonga, R. Romijnders, F. Hubis, X. Zhai, N. Houlsby, D. Tran, and M. Lucic, “Revisiting the calibration of modern neural networks,” *Advances in Neural Information Processing Systems*, vol. 34, pp. 15 682–15 694, 2021.
- [49] M. P. Naeini, G. Cooper, and M. Hauskrecht, “Obtaining well calibrated probabilities using bayesian binning,” in *Proceedings of the AAAI conference on artificial intelligence*, vol. 29, no. 1, 2015.
- [50] J. Nixon, M. W. Dusenberry, L. Zhang, G. Jerfel, and D. Tran, “Measuring calibration in deep learning,” in *CVPR workshops*, vol. 2, no. 7, 2019.
- [51] V. Kuleshov, N. Fenner, and S. Ermon, “Accurate uncertainties for deep learning using calibrated regression,” in *International conference on machine learning*. PMLR, 2018, pp. 2796–2804.
- [52] A. P. Dawid, “Statistical theory: The prequential approach (with discussion and rejoinder),” *Journal of the Royal Statistical Society, Series A*, vol. 147, pp. 278–292, 1984.
- [53] S. Young and P. Jenkins, “On measuring calibration of discrete probabilistic neural networks,” 2024.
- [54] T. Gneiting and A. E. Raftery, “Strictly proper scoring rules, prediction, and estimation,” *Journal of the American statistical Association*, vol. 102, no. 477, pp. 359–378, 2007.
- [55] T. Gneiting, F. Balabdaoui, and A. E. Raftery, “Probabilistic forecasts, calibration and sharpness,” *Journal of the Royal Statistical Society Series B: Statistical Methodology*, vol. 69, no. 2, pp. 243–268, 2007.
- [56] Mixture distribution. [Online]. Available: [https://en.wikipedia.org/wiki/Mixture\\_distribution](https://en.wikipedia.org/wiki/Mixture_distribution)
- [57] J. S. Marron and M. P. Wand, “Exact mean integrated squared error,” *The Annals of Statistics*, vol. 20, no. 2, pp. 712–736, 1992.
- [58] A. Paszke, S. Gross, S. Chintala, G. Chanan, E. Yang, Z. DeVito, Z. Lin, A. Desmaison, L. Antiga, and A. Lerer, “Automatic differentiation in pytorch,” 2017.
- [59] J. Q. Candela, C. E. Rasmussen, F. H. Sinz, O. Bousquet, and B. Schölkopf, “Evaluating predictive uncertainty challenge,” in *MLCW*, 2005, pp. 1–27.
- [60] H. Fanaee-T and J. Gama, “Event labeling combining ensemble detectors and background knowledge,” *Progress in Artificial Intelligence*, vol. 2, pp. 113–127, 2014.
- [61] U. K. D. for Transport, “Road safety data,” 2022.
- [62] T.-Y. Lin, M. Maire, S. Belongie, J. Hays, P. Perona, D. Ramanan, P. Dollár, and C. L. Zitnick, “Microsoft coco: Common objects in context,” in *Computer Vision–ECCV 2014: 13th European Conference, Zurich, Switzerland, September 6–12, 2014, Proceedings, Part V 13*. Springer, 2014, pp. 740–755.

- [63] B. Wu, C. Xu, X. Dai, A. Wan, P. Zhang, Z. Yan, M. Tomizuka, J. Gonzalez, K. Keutzer, and P. Vajda, “Visual transformers: Token-based image representation and processing for computer vision,” 2020.
- [64] J. Deng, W. Dong, R. Socher, L.-J. Li, K. Li, and L. Fei-Fei, “Imagenet: A large-scale hierarchical image database,” in *2009 IEEE conference on computer vision and pattern recognition*. Ieee, 2009, pp. 248–255.
- [65] J. Ni, J. Li, and J. McAuley, “Justifying recommendations using distantly-labeled reviews and fine-grained aspects,” in *Proceedings of the 2019 conference on empirical methods in natural language processing and the 9th international joint conference on natural language processing (EMNLP-IJCNLP)*, 2019, pp. 188–197.
- [66] V. Sanh, L. Debut, J. Chaumond, and T. Wolf, “Distilbert, a distilled version of bert: smaller, faster, cheaper and lighter,” *ArXiv*, vol. abs/1910.01108, 2019.
- [67] *The Holy Bible: King James Version*. Cambridge University Press, 2021.
- [68] ebible. [Online]. Available: <https://github.com/BibleNLP/ebible>
- [69] C. E. Shannon, “A mathematical theory of communication,” *The Bell system technical journal*, vol. 27, no. 3, pp. 379–423, 1948.
- [70] P. Good, *Permutation tests: a practical guide to resampling methods for testing hypotheses*. Springer Science & Business Media, 2013.
- [71] J. Kiefer and J. Wolfowitz, “Stochastic estimation of the maximum of a regression function,” *The Annals of Mathematical Statistics*, pp. 462–466, 1952.
- [72] D. P. Kingma and J. Ba, “Adam: A method for stochastic optimization,” *arXiv preprint arXiv:1412.6980*, 2014.
- [73] I. Loshchilov and F. Hutter, “Decoupled weight decay regularization,” *arXiv preprint arXiv:1711.05101*, 2017.
- [74] K. Fukushima, “Visual feature extraction by a multilayered network of analog threshold elements,” *IEEE Transactions on Systems Science and Cybernetics*, vol. 5, no. 4, pp. 322–333, 1969.
- [75] T. Hill, “Conflations of probability distributions,” *Transactions of the American Mathematical Society*, vol. 363, no. 6, pp. 3351–3372, 2011.
- [76] I. Loshchilov and F. Hutter, “Sgdr: Stochastic gradient descent with warm restarts,” *arXiv preprint arXiv:1608.03983*, 2016.
- [77] E. D. Cubuk, B. Zoph, D. Mane, V. Vasudevan, and Q. V. Le, “Autoaugment: Learning augmentation policies from data,” *arXiv preprint arXiv:1805.09501*, 2018.

## A Deep Double Poisson Networks (DDPNs)

### A.1 Limitations

DDPNs are general, easy to implement, and can be applied to a variety of datasets. However, some limitations do exist. One limitation that might arise is on count regression problems of very high frequency (i.e., on the order of thousands or millions). In this paper, we don't study the behavior of DDPN relative to existing benchmarks on high counts. In this scenario, it is possible that the choice of a Gaussian as the predictive distribution may offer a good approximation, even though the regression targets are discrete.

We also note that the general approximations  $\mathbb{E}[Z] \approx \mu$  and  $\text{Var}[Z] \approx \frac{\mu}{\phi}$  for some  $Z \sim \text{DP}(\mu, \phi)$  we employ in this work have not been extensively studied. It is possible that there are edge cases where these estimates diverge from the true moments of the distribution.

One difficulty that can sometimes arise when training a DDPN is poor convergence of the model weights. In preliminary experiments for this research, we had trouble obtaining consistently high-performing solutions with the SGD [71] and Adam [72] optimizers, thus AdamW [73] was used instead. Future researchers using the DDPN technique should be wary of this behavior.

In this paper, we performed a single out-of-distribution (OOD) experiment on Amazon Reviews. This experiment provided encouraging evidence of the efficacy of DDPN for OOD detection. However, the conclusions drawn from this experiment may be somewhat limited in scope since the experiment was performed on a single dataset and task. Future work should seek to build off of these results to more fully explore the OOD properties of DDPN on other count regression tasks.

### A.2 Deriving the DDPN Objective

This loss function is obtained by first noting that

$$\begin{aligned}
 \max_{\Theta} \left[ \frac{1}{N} \sum_{i=1}^N p(y_i | \mathbf{f}_{\Theta}(\mathbf{x}_i)) \right] &= \max_{\Theta, \mu, \phi} \left[ \frac{1}{N} \sum_{i=1}^N p(y_i | \mu_i, \phi_i) \right] \\
 &= \min_{\Theta, \mu, \phi} \left[ -\frac{1}{N} \sum_{i=1}^N \log(p(y_i | \mu_i, \phi_i)) \right] \\
 &= \min_{\Theta, \mu, \phi} \left[ -\frac{1}{N} \sum_{i=1}^N \log \left( \phi_i^{\frac{1}{2}} e^{-\phi_i \mu_i} \left( \frac{e^{-y_i} y_i^{y_i}}{y_i!} \right) \left( \frac{e \mu_i}{y_i} \right)^{\phi_i y_i} \right) \right] \\
 &= \min_{\Theta, \mu, \phi} \left[ -\frac{1}{N} \sum_{i=1}^N \log \left( \phi_i^{\frac{1}{2}} e^{-\phi_i \mu_i} \left( \frac{e \mu_i}{y_i} \right)^{\phi_i y_i} \right) \right] \\
 &= \min_{\Theta, \mu, \phi} \left[ -\frac{1}{N} \sum_{i=1}^N \left( \frac{1}{2} \log \phi_i - \phi_i \mu_i + \phi_i y_i (1 + \log \mu_i - \log y_i) \right) \right]
 \end{aligned}$$

Thus,

$$\mathcal{L}_{DDPN}(y_i, \mu_i, \phi_i) = \frac{1}{N} \sum_{i=1}^N \left( -\frac{1}{2} \log \phi_i + \phi_i \mu_i - \phi_i y_i (1 + \log \mu_i - \log y_i) \right) \quad (6)$$

### A.3 DDPN Ensembles

In Section 3.3 we describe how the ensembled predictive distribution is a uniform mixture of the  $M$  members of the ensemble:

$$p(y_i|\mathbf{x}_i) = \frac{1}{M} \sum_{m=1}^M p(y_i|\mathbf{f}_{\Theta_m}(\mathbf{x}_i)) \quad (7)$$

Letting  $\mu_m = \mathbb{E}[y_i|\mathbf{f}_{\Theta_m}(\mathbf{x}_i)]$  and  $\sigma_m^2 = \text{Var}[y_i|\mathbf{f}_{\Theta_m}(\mathbf{x}_i)]$ , we can get the mean and variance of the predictive distribution as follows:

$$\mathbb{E}[y_i|\mathbf{x}_i] = \frac{1}{M} \sum_{m=1}^M \mu_m, \quad \text{Var}[y_i|\mathbf{x}_i] = \sum_{m=1}^M \frac{\sigma_m^2 + \mu_m^2}{M} - \left( \sum_{m=1}^M \frac{\mu_m}{M} \right)^2 \quad (8)$$

We note that this same technique can be applied to form an ensemble from any collection of neural networks outputting a discrete distribution, regardless of the specific parametric form [56, 57].

## B Detailed Description of Experiments

In all experiments, instead of using the final set of weights achieved during training with a particular technique, we selected the weights associated with the best mean absolute error (MAE) on a held-out validation set. This can be viewed as a form of early stopping, since models were observed to eventually overfit to the training data on almost every dataset we tested.

We note that when a point prediction was required, such as for computing the MAE of a model, we took the mode of the posterior predictive distribution instead of the mean. When the mode was not an integer (e.g. in the Gaussian case), we rounded to the nearest integer.

The ReLU [74] activation was exclusively used for all MLPs. No dropout or batch normalization was applied.

### B.1 Simulation Experiment

This dataset is generated with the following procedure: First, we sample  $x$  from a uniform distribution,  $x \sim \text{Uniform}(0, 2\pi)$ . Next, we draw an initial proposal for  $y$  from a conflation [75] of five identical Poissons, each with rate parameterized by  $\lambda(x) = 10 \sin(x) + 10$ . We scale  $y$  by  $-1$  and shift it by  $+30$  to force over-dispersion at low counts and under-dispersion at high counts while maintaining nonnegativity.

Each MLP (with layers of width [128, 128, 128, 64]) was trained for 200 epochs on the CPU of a 2021 MacBook Pro with a batch size of 32 using the AdamW optimizer [73]. The initial learning rate was set to  $10^{-3}$  and annealed to 0 with a cosine schedule [76], and weight decay was set to  $10^{-5}$ .

### B.2 Tabular Datasets

#### B.3 Bikes

In this experiment, each regression head was placed on top of an MLP with layers of width [128, 128, 128, 64]. Models were trained for 100 epochs on the CPU of a 2021 MacBook Pro with the AdamW optimizer, using a batch size of 128. The initial learning rate was  $10^{-3}$ , decayed to 0 following a cosine schedule. Weight decay was set to  $10^{-5}$ . For continuous features such as temperature, model inputs were standardized to have a mean of 0 and a standard deviation of 1. The season, mnth, and hr columns were transformed using a trigonometric encoding procedure.

Due to the higher counts in this dataset, and to facilitate a fairer comparison, for the Gaussian DNN, Stirn, and Seitzer techniques, we reconfigured the model to output  $[\log \hat{\mu}_i, \log \hat{\sigma}_i^2]^T$  instead of  $[\hat{\mu}_i, \log \hat{\sigma}_i^2]^T$ . We observed a great performance boost with this adjustment.

We used the Bikes dataset under the Creative Commons Attribution 4.0 International (CCBY 4.0) license. The source URL is <https://archive.ics.uci.edu/dataset/275/bike+sharing+dataset>.



## B.4 Collisions

We formed the Collisions dataset by joining the “Casualties”, “Collisions”, and “Vehicles” tables on the `accident_reference` column. Feature engineering included merging all associated data from a specific collision into a single row (by creating columns for each feature of each vehicle involved in the collision, for example) and one-hot encoding all categorical variables. The MLP used for feature extraction had layer widths of [1630, 512, 256, 256, 128, 128, 128, 64]. Models were trained on a 2021 MacBook Pro CPU for 100 epochs with a batch size of 32. The AdamW optimizer was used, with an initial learning rate of  $10^{-5}$  and a cosine decay to 0.

The Collisions dataset is published by the United Kingdom’s Department for Transport, and we used it under the Open Government Licence. The URL where this data is hosted is <https://www.data.gov.uk/dataset/cb7ae6f0-4be6-4935-9277-47e5ce24a11f/road-safety-data>.

## B.5 Vision Datasets

### B.5.1 COCO-People

All networks were trained for 30 epochs (updating all weights, including the ViT backbone) using the AdamW optimizer with an initial learning rate of  $10^{-3}$  and weight decay of  $10^{-5}$ . The learning rate was decayed to 0 with a cosine schedule. The regression head on top of the ViT backbone was a two-layer MLP with layer widths [384, 256]. Models were trained in a distributed fashion across 4 Nvidia L4 Tensor Core GPUs on a Google Cloud Platform (GCP) VM instance, with an effective batch size of 256. Images were normalized with the ImageNet [64] pixel means and standard deviations and augmented during training with the AutoAugment transformation [77]. Training was done with BFloat 16 Mixed Precision.

The COCO dataset from which we formed the COCO-People subset is distributed via the CCBY 4.0 license. It can be accessed at <https://cocodataset.org/#home>.

### B.5.2 Inventory

Networks were trained with the AdamW optimizer for 50 epochs with an initial learning rate of  $10^{-3}$  and weight decay of  $10^{-5}$ . Cosine annealing was used to decay the learning rate to 0. An effective batch size of 16 was used, split across an internal cluster of 4 NVIDIA GeForce RTX 2080 Ti GPUs.

The Inventory dataset was made available to us via an industry collaboration and is not publicly accessible.

## B.6 Text Dataset

### B.6.1 Amazon Reviews

All networks were trained for 10 epochs across 8 Nvidia L4 Tensor Core GPUs (on a GCP VM instance) with an effective batch size of 2048. The AdamW optimizer was used for training, with an initial learning rate of  $10^{-4}$  (annealed to 0 with a cosine schedule) and weight decay of  $10^{-5}$ . Training was done with BFloat 16 Mixed Precision. Both the feature extractor, DistilBERT [66], and the MLP regression head (with layer widths [384, 256]) were updated during training.

Amazon Reviews is publicly available (with a citation, which we provide in the body of the paper) at [https://cseweb.ucsd.edu/~jmcauley/datasets/amazon\\_v2/](https://cseweb.ucsd.edu/~jmcauley/datasets/amazon_v2/). The “Patio, Lawn, and Garden” subset we employ in this work is accessible at [https://datarepo.eng.ucsd.edu/mcauley\\_group/data/amazon\\_v2/categoryFilesSmall/Patio\\_Lawn\\_and\\_Garden.csv](https://datarepo.eng.ucsd.edu/mcauley_group/data/amazon_v2/categoryFilesSmall/Patio_Lawn_and_Garden.csv).

## B.7 Out-of-distribution Behavior

We run a one-sided, two-sample permutation test [70] using the difference of means as our test statistic. Given samples  $S_{ID}$  and  $S_{OOD}$  with respective means  $\bar{x}_{ID}$  and  $\bar{x}_{OOD}$ , we define  $\Delta = \bar{x}_{OOD} - \bar{x}_{ID}$ . We then take  $n = 1500$  permutations of  $S_{ID}$  and  $S_{OOD}$  and compute  $\Delta^{(i)} = \bar{x}_{OOD}^{(i)} - \bar{x}_{ID}^{(i)}$  for each permutation  $i \in \{1, 2, \dots, n\}$ . We take  $p = \frac{|\{i \mid \Delta^{(i)} > \Delta\}|}{n}$  to be the proportion of permutations yielding a greater difference of means than  $\Delta$ . In a formal sense, if we define the null hypothesis

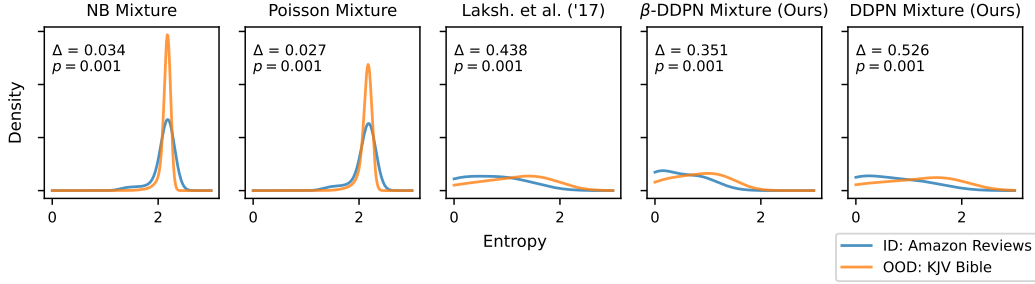


Figure 4: In-distribution (ID) vs. out-of-distribution (OOD) behavior for ensembles of regression models trained on Amazon Reviews. We plot the KDE-smoothed distributions of entropy values obtained from the ID (Amazon Reviews) and OOD (KJV Bible) datasets (see Section 4.5 for more details). We also perform a two-sample permutation test with the difference-of-means statistic ( $\Delta$ ) and display the statistic, along with the p-value from the test, on the corresponding plot for each ensemble model. Just like in the individual case, ensembles of DDPN models exhibit the largest gap in entropy between ID and OOD data.

$H_0 : \Delta \leq 0$  and the alternative hypothesis  $H_1 : \Delta > 0$ , we may treat  $p$  as an estimate of  $P(S_{ID}, S_{OOD} | H_0)$ . Higher entropy indicates higher uncertainty / expected chaos in a model’s predictive distributions. Thus, we expect that the models most able to distinguish between ID / OOD will have the highest  $\Delta$  (since their mean entropy should be higher on OOD than on ID).

## C Additional Case Studies

### C.1 Case studies on COCO-People

In this section we perform multiple case studies of the behavior of different heteroscedastic regressors on COCO-People. In Figure 5 we display three examples from the COCO-People test set and plot the corresponding predictive distributions produced by  $\beta$ -DDPN. We see varying ranges of predictive uncertainty, while in each case the ground truth count is contained within the predictive HDI.

We next perform a side-by-side comparison of a variety of methods in Figure 6. We display a number of both single forward pass and ensemble methods, plotting their predictive distributions on example images from the test set.

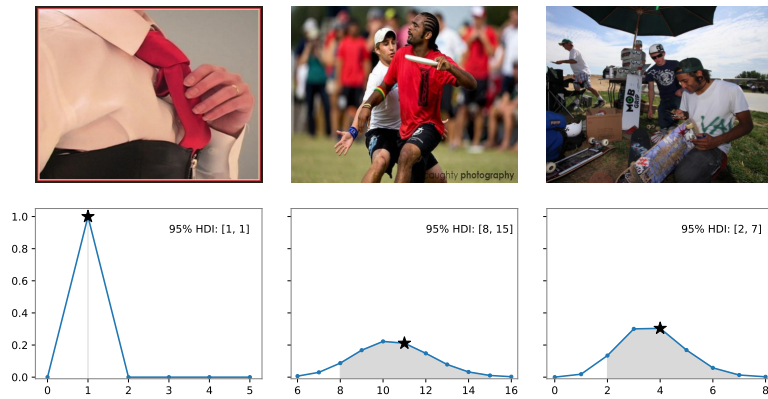


Figure 5: Example  $\beta$ -DDPN predictive distributions on COCO-People. The network is able to flexibly represent counts of different magnitudes with varying degrees of uncertainty, as desired.

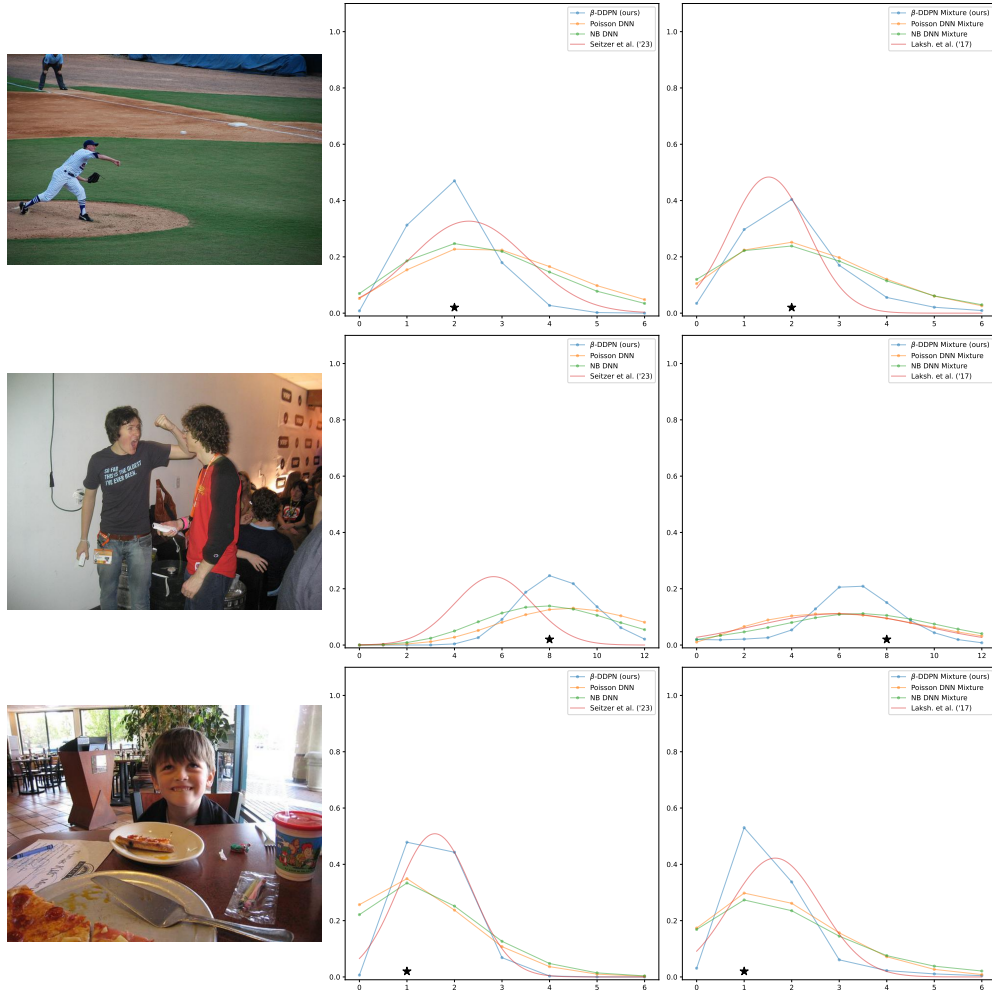


Figure 6: More example predictive distributions on COCO-People. The second column shows distributions output by individual models, while the third column shows outputs from various ensembling techniques. For the sake of visual clarity, for the Double Poisson and Gaussian models, only the best-performing method is shown.

## C.2 Case studies on Amazon Reviews

In this section we perform a case study of each heteroscedastic method trained on Amazon Reviews. We randomly sample four examples from the test split of Amazon Reviews. We also sample four random verses from the English KJV Bible. Then, for each method, we plot the predictive distribution of the respective regressor. See Figures 7,8,9,10, 11,12, 13, and 14.

A major insight we have from this case study is that, in addition to its strong quantitative performance exhibited in Section 4.5, DDPN appears to provide the best qualitative OOD behavior. In Figure 7 we observe that DDPN exhibits ideal behavior in-distribution with different predictive distributions for reviews with varying valence. However, when fed verses from the KJV Bible, the resulting predictive distributions are essentially the same: diffuse and uninformative across the domain of reviews. In fact, this is evidence that DDPNs revert to the Optimal Constant Solution (OCS) identified by [7] better than existing methods.

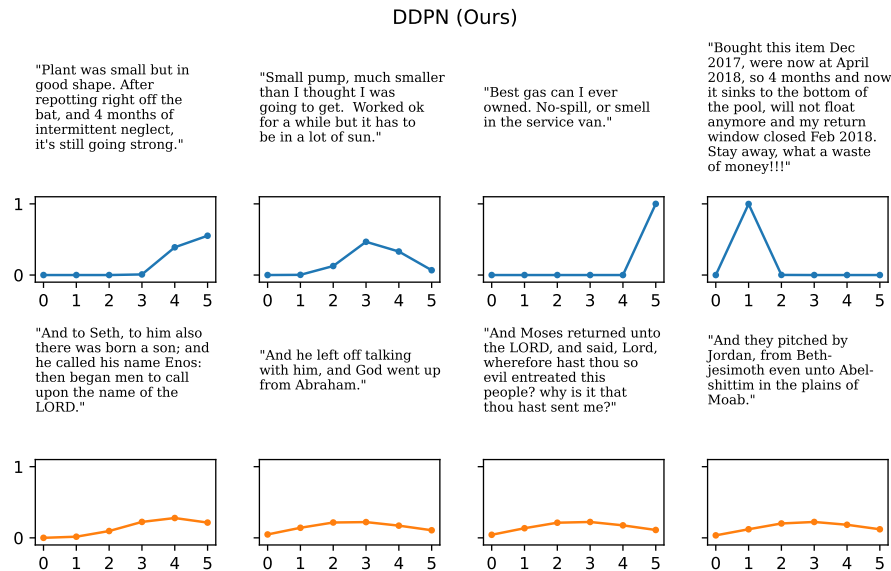


Figure 7: Predictive distributions produced by DDPN on four randomly sampled examples from Amazon Reviews and the KJV Bible. DDPN exhibits ideal behavior in-distribution with different predictive distributions for reviews with varying valence. For the KJV Bible, the resulting predictive distributions are essentially the same across examples: diffuse and uninformative. This suggests that DDPNs revert to the Optimal Constant Solution (OCS) identified by [7] better than existing methods.

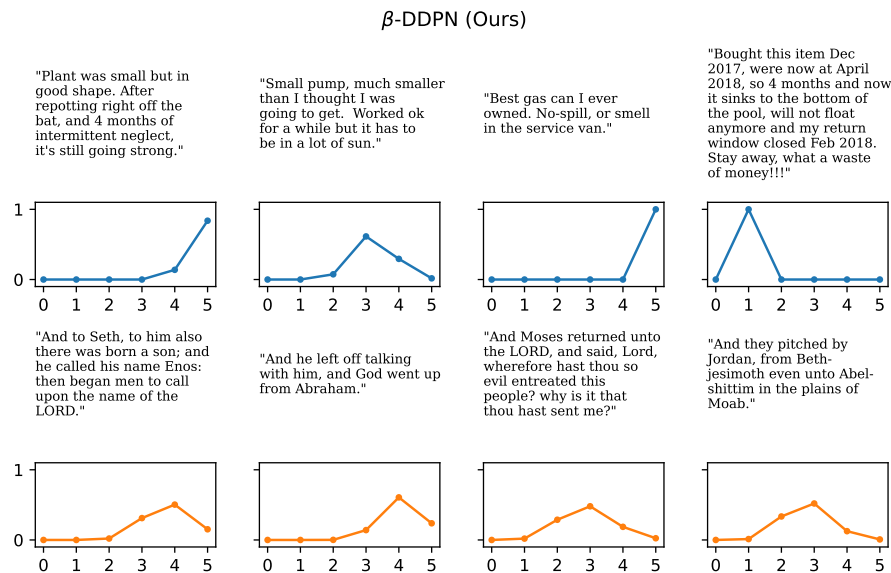


Figure 8: Predictive distributions produced by  $\beta$ -DDPN on four randomly sampled examples from Amazon Reviews and the KJV Bible.

Stirn et al. ('23)

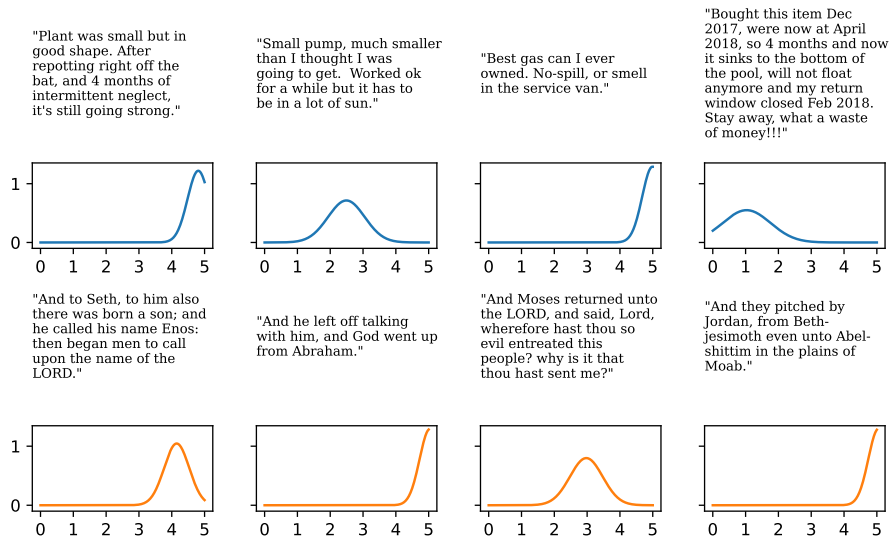


Figure 9: Predictive distributions produced by Stirn et al. on four randomly sampled examples from Amazon Reviews and the KJV Bible.

Immer et al. ('23)

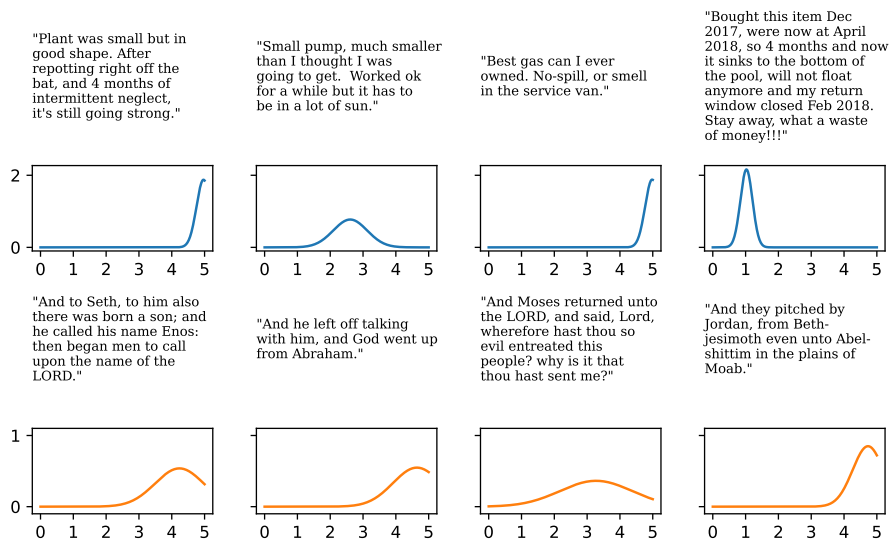


Figure 10: Predictive distributions produced by Immer et al. on four randomly sampled examples from Amazon Reviews and the KJV Bible.

Seitzer et al. ('23)

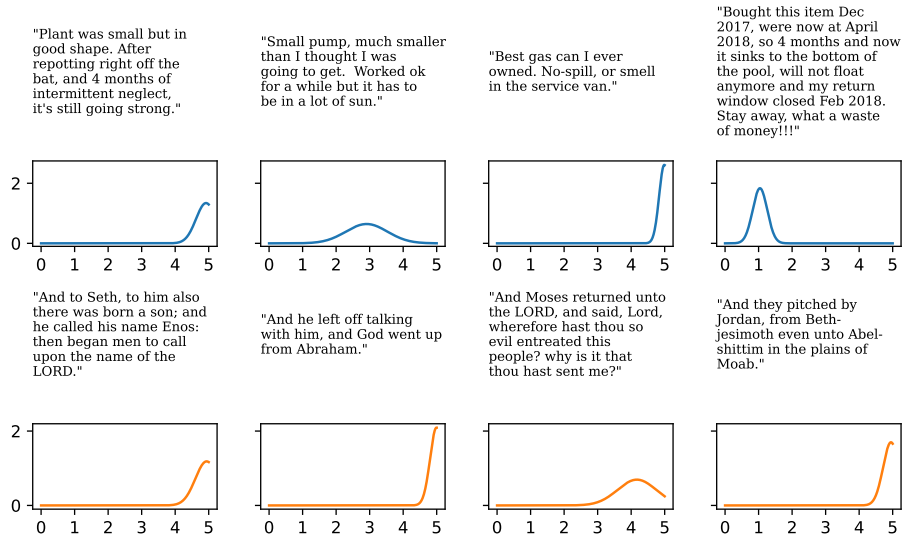


Figure 11: Predictive distributions produced by Seitzer et al. on four randomly sampled examples from Amazon Reviews and the KJV Bible.

Gaussian DNN

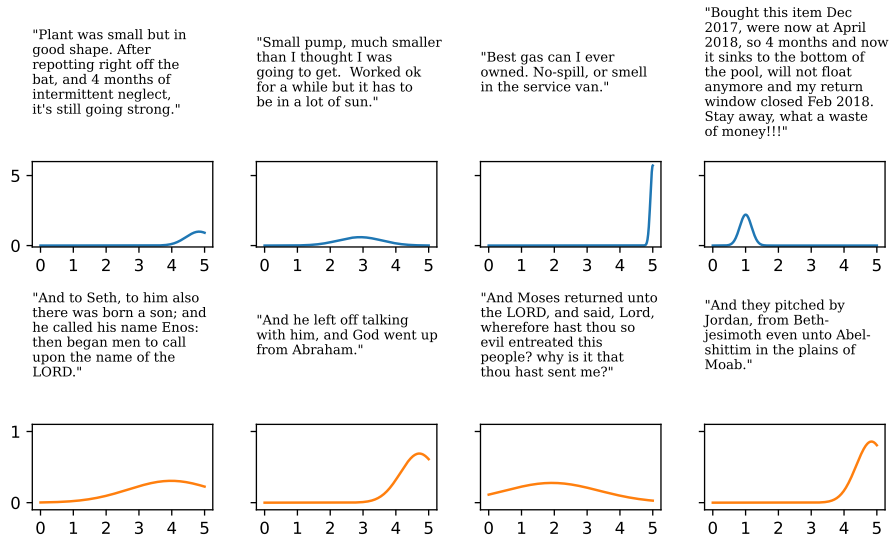


Figure 12: Predictive distributions produced by Gaussian DNN on four randomly sampled examples from Amazon Reviews and the KJV Bible.

NB DNN

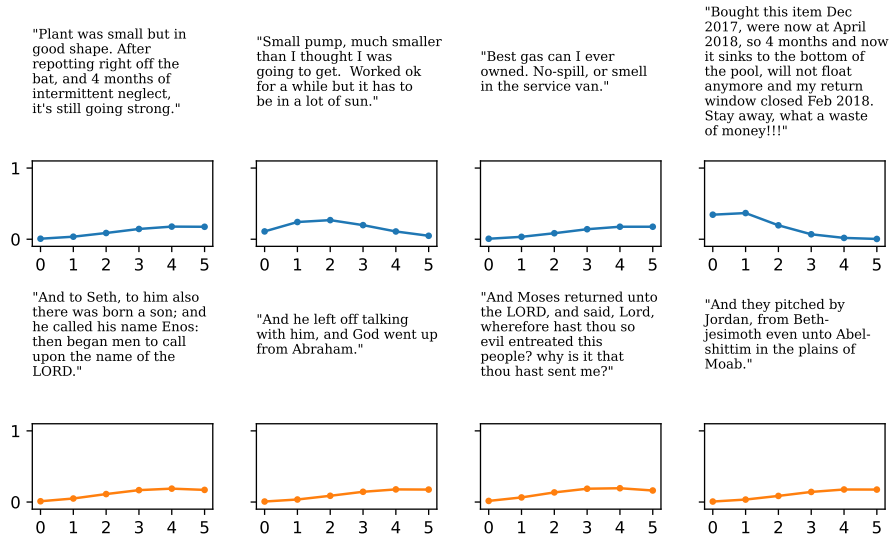


Figure 13: Predictive distributions produced by NB DNN on four randomly sampled examples from Amazon Reviews and the KJV Bible.

Poisson DNN

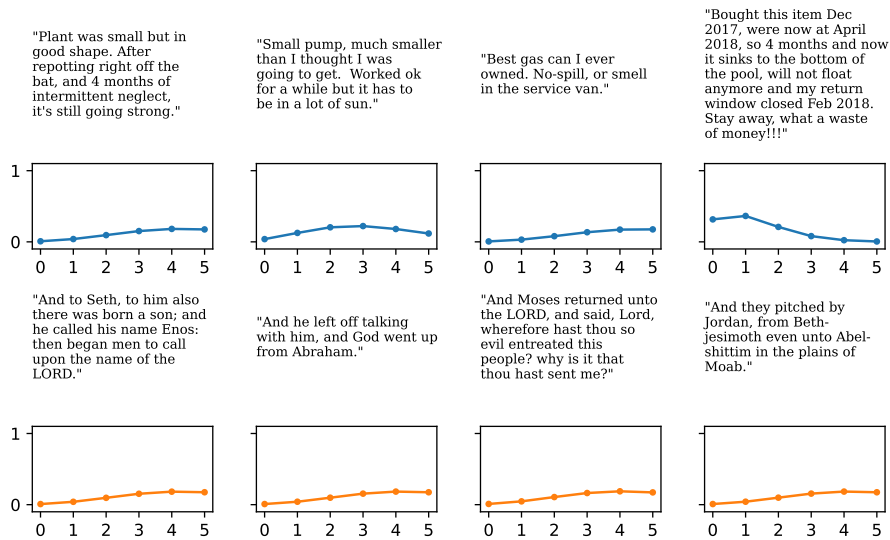


Figure 14: Predictive distributions produced by Poisson DNN on four randomly sampled examples from Amazon Reviews and the KJV Bible.

## D Example Point Cloud from Inventory

In Figure 15, we provide an example point cloud from the Inventory dataset used in the experiments of Section 4.3. Further examples can be viewed in [24].

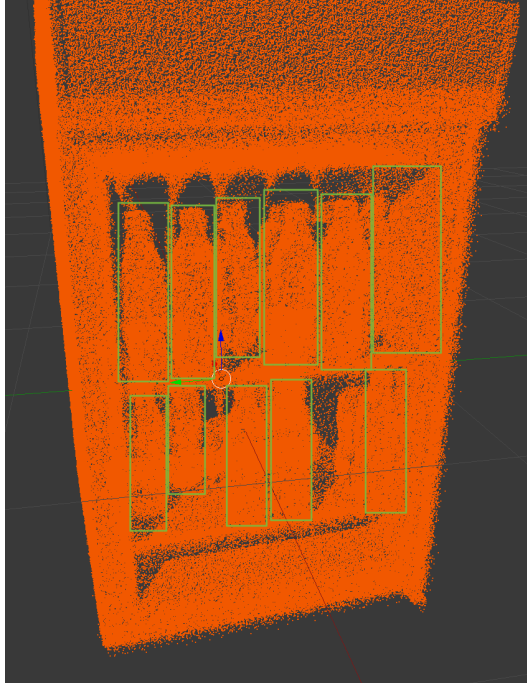


Figure 15: Example point cloud from Inventory. Each green box represents an inventory slot which is segmented into a point beam (see [24] for details and further examples). Models predict the product count within each point beam.